Journal of the Brazilian Society of Mechanical Sciences and Engineering (2024) 46:76
https://doi.org/10.1007/s40430-023-04662-4

TECHNICAL PAPER

Pilot injection impact on diesel PCCI combustion: an endoscopic study with a turbocharged engine

Huaping Xu[1,2] · Xuedong Wu[1] · Hekun Jia[2]

Received: 24 July 2022 / Accepted: 17 December 2023 / Published online: 14 January 2024

Abstract

In this study, the effects of pilot injection on premixed charge compression ignition were investigated in a turbocharged diesel engine equipped with an endoscopic visualization system, and experiments were conducted under a speed of 1450 rpm at 25% and 50% loads. Results indicated that as the pilot injection mass and timing increased, the diffusion flame advanced and the flame area expanded. However, when the pilot timing advanced to 70 °BTDC, the flame luminance remained nearly constant. Moreover, with increased pilot injection mass, the peak values of in-cylinder pressure and the heat release rate of the pilot injection combustion were increased, brake-specific fuel consumption (BSFC) slightly increased, soot initially decreased but then increased, nitrogen oxide (NO_X) was reduced by a maximum of 54%. The in-cylinder pressure peak value decreased with the advance of pilot injection timing, and the main combustion exhibited a lower heat release rate. Nevertheless, NO_X increased significantly, and soot decreased initially but showed a slight increase at 25% load. RSM was used for finding the optimal pilot injection strategy to minimize BSFC and emissions. The optimal values found were a pilot injection timing of 50 °BTDC and a pilot injection mass of 4.4 mg for 25% load, and corresponding values of 58.9 °BTDC and 5.5 mg for 50% load.

Keywords PCCI · Diesel engine · Endoscope · Emissions

1 Introduction

Direct injection (DI) diesel engines, known for their high thermal efficiency and reliability, have found extensive use in automobiles and various industrial applications, despite the challenges posed by fuel cells and electric vehicles [1]. To meet increasingly stringent emission regulations, advanced combustion modes like Homogeneous Charge Compression Ignition (HCCI) [2], premixed charge compression ignition (PCCI), and Reactivity-Controlled Compression Ignition (RCCI) [3, 4] were developed to create homogeneous air–fuel mixtures and optimize the combustion process. Among these combustion concepts, PCCI stands out due to its minimal to zero engine modification requirements [5]. This, combined with its exceptional fuel adaptability and low combustion noise, has resulted in its widespread adoption within the diesel engine sector.

PCCI combustion, positioned between HCCI and conventional combustion, relies on early injection, high fuel injection pressure, and exhaust gas recirculation (EGR) for its operation [6]. Due to the relatively simple injection pressure and EGR control, PCCI combustion research has predominantly concentrated on injection strategies. Jia et al. [7] investigated the impact of injection timings on the combustion and emission characteristics of a diesel-fueled PCCI engine. Their findings demonstrated that optimized injection timings led to a significant reduction in NOx emissions due to low-temperature combustion (LTC). Zehni et al. [8] showed numerically that early injection timing results in lower maximum local equivalence ratios in PCCI combustion, thereby reducing HC and CO emissions. However, excessively early injection timings can lead to fuel spray impingement on the cylinder walls, causing cylinder wall wetting, incomplete combustion, and subsequently, reduced power output and higher emissions. To mitigate wall wetting,

Technical Editor: Mario Eduardo Santos Martins.

✉ Huaping Xu
xhp@just.edu.cn

[1] School of Energy and Power Engineering, Jiangsu University of Science and Technology, Zhenjiang, China

[2] School of Automotive and Traffic Engineering, Jiangsu University, Zhenjiang, China

researchers have explored the use of small cone angle nozzles (within 100°) [9]. These nozzles increase the distance between the nozzle and cylinder wall, promoting greater fuel atomization before entry into the cylinder. Nevertheless, the effectiveness of this approach is limited. Early injection timings introduce additional challenges. Horbe et al. [10] conducted PCCI experiments with early injection and observed lower NOx and PM emissions alongside higher brake thermal efficiency (BTE). However, they noted that the higher rate of pressure rise reduced the operational range of PCCI combustion.

To address these issues, researchers have implemented pilot injection strategies. The pilot injection coupled with proper main injection timing diminishes the average in-cylinder temperature for decreasing NO_X emission. On the other hand, pilot injection will cause a higher maximum temperature before main injection, and lean burn zone compared to single injection. The reason is because the combustion of pilot injection fuel could increase the temperature in-cylinder before main injection. When the fuel of main injection enters the high temperature zone during the main injection, the fuel combustions more quickly, so polycyclic aromatic hydrocarbons (PAHs) formation rates reduce [11]. Cao et al. [12] observed that pilot injection enhances the flame propagation speed of the main injection, resulting in a more uniform distribution of soot concentration. They also noted the sensitivity of ignition delay to pilot injection timing and the enhancement of main combustion with higher pilot injection mass. Lu et al. [6] conducted numerical simulations on the pilot injection strategy of a PCCI diesel engine. By optimizing the pilot injection strategy at an engine speed of 1000 r/min, they achieved a remarkable 38.5% reduction in NOx emissions and a one-order-of-magnitude decrease in soot emissions. Additionally, the gross indicated thermal efficiency increased by 8.66%. Herfatmanesh et al. [13] revealed that the use of pilot injection led to reductions in both soot and NOx emissions but resulted in an approximately 26% increase in Unburned Hydrocarbon (UHC) emissions. Qiu et al. [14] conducted experimental research to investigate various pilot injection strategies. Their findings indicated that advancing pilot injection timing led to a decrease in peak in-cylinder pressure and ignition delay. Moreover, an increase in pilot injection fuel mass resulted in higher heat release rates during pilot injection combustion and an increased maximum rate of pressure rise. However, one study discovered that when the pilot injection mass ratio exceeded 40%, the brake mean effective pressure (BMEP) significantly decreased [15]. Wang et al. [16] conducted matching tests between multiple injection strategies and different typical working conditions of a diesel engine. Their results demonstrated that significant reductions in NOx and soot emissions could be achieved when a diesel engine operated under low-speed, low-load conditions, especially when using a combination of a large pilot-main interval and a small pilot injection mass. Huang et al. [17] found that a small pilot-main interval could decrease energy loss, CO emissions, and improve BTE. Furthermore, pilot injections are effective in reducing combustion noise, particularly at engine idle [18], with reductions of up to 5–8 dB generally obtained when compared to single injection strategies [19].

Prior research has extensively investigated the impact of pilot injection strategies in PCCI combustion conditions. However, these studies have primarily focused on macro-level performance aspects of diesel engines, neglecting detailed analysis of in-cylinder visualizations pertaining to spray formations, mixture compositions, and combustion characteristics. In order to bridge this gap, the present experimental study adopts a unique approach by employing endoscopic visualization techniques to examine spatial distribution of both spray patterns and flame propagation in a diesel engine. Notably, unlike optical engines, the endoscopic visualization system enables assessments without necessitating extensive engine modifications that could potentially alter in-cylinder mixing and combustion. In addition to these visual assessments, the study also encompasses analysis of key engine performance parameters including in-cylinder pressure, heat release rate, fuel consumption, and emissions, as well as optimization of pilot injection parameters. These comprehensive investigations aim to provide valuable insights into the effects of pilot injection strategies on both micro-scale in-cylinder phenomena and overall engine performance.

2 Experimental apparatus and procedures

2.1 Experimental setup

The main specifications of the test engine are listed in Table 1. The test engine is an inline four-cylinder, four-stroke, turbocharged diesel engine, fitted with a Bosch Common Rail injection system. In order to capture the real-time combustion flame in cylinder, the test engine was equipped

Table 1 The main specifications of the test engine

Description	Specification
Engine type	Four-cylinder diesel engine
Bore (mm)	95
Stroke (mm)	100
Compression ratio	17.5
Displacement (*L*)	2.83

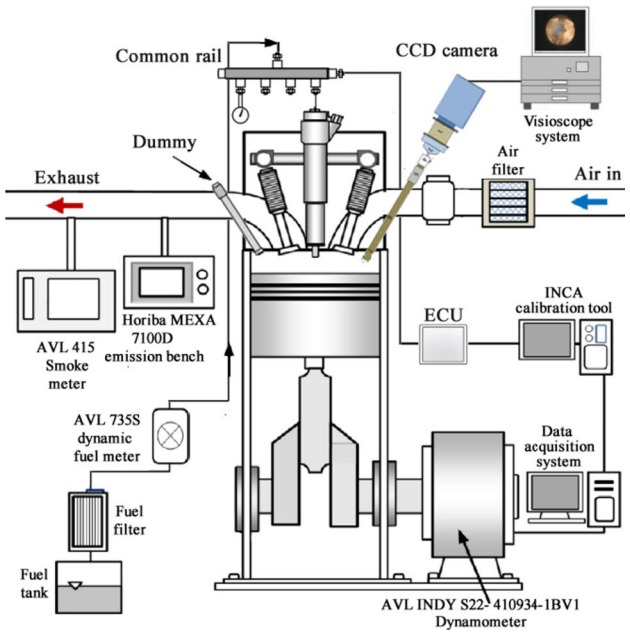

Fig. 1 Schematic diagram of test system

with an endoscopic visualization system through the engine cylinder head.

Schematic of test system is indicated in Fig. 1. The injection parameters were controlled by using calibration software (ETAS INCA 6.2). The in-cylinder pressure was measured by a piezoelectric pressure transducer (Kistler 6125B01). Through the in-cylinder pressure data, the HRR was calculated on the basis of the First Law of Thermodynamics. Fuel consumption was measured using a gravimetric fuel flow meter (AVL 735S). The exhaust gases emissions were detected with the HORIBA MEXA-7200D. The exhaust soot was obtained by a smoke analyzer (AVL 415S) that displays results directly in Filter Smoke Number (FSN), and the FSN value can be converted into unit g/h using an empirical equation obtained from AVL [20]. The accuracies and uncertainties of the measuring instruments utilized in this study are shown in Table 2.

2.2 Endoscopic visualization system

Combustion visualization was performed by using AVL 513D Visioscope. This endoscopic visualization system includes an endoscope, a high-speed CCD camera, a lighting device and AVL's Thermo Vision program. The first cylinder head has been modified to obtain an optical path into the combustion chamber. Figure 2 indicates that two holes were machined in the first cylinder head for inserting the endoscope and lighting device, and the bowl-in-piston was also modified in order to avoid close contact between the components inserted and the reciprocating piston, as shown in the right side of Fig. 2.

Figure 3 shows the schematic diagram of endoscopic measurement. Additionally, the introduction of cool air significantly enhances the endoscope's capacity to withstand elevated thermal loads. The high-speed CCD Camera provides 640×480 pixel resolution at a frequency of 10 Hz. The CCD camera and the lighting device were synchronized to

Table 2 Accuracies and uncertainties of the measurement instruments

	Measuring instruments	Range	Accuracy	Uncertainty
Dynamometer	AVL INDYS22-410,934-1BV-1	Speed: 0–7000 r/min Torque: 0–1400 N m	Speed: ± 1 r/min Torque: ± 0.5% F.S	± 0.4% ± 0.4%
Fuel flow meter	AVL 735S	0–125 kg/h	± 0.12%	± 1.0%
NO_X	HORIBA MEXA 7100D	0–10 ~ 500,1000 ~ 10,000 ppm	± 1 ppm	± 1.0%
Soot	AVL 415S	0–10 FSN	± 1%	0.005 FSN + 3% of measured value

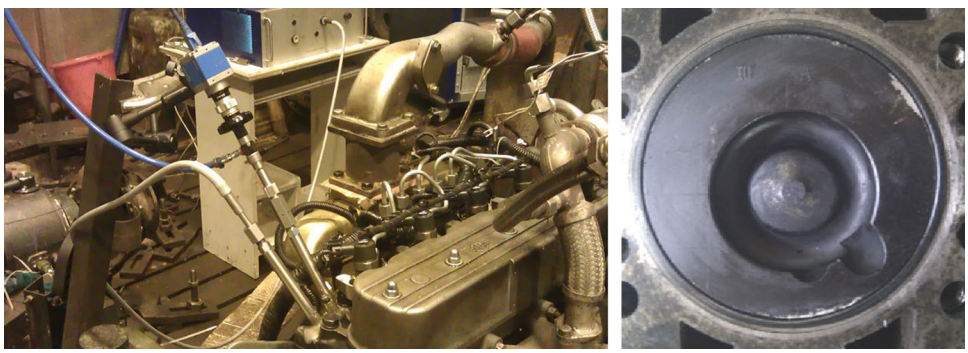

Fig. 2 Endoscope system and modified cylinder piston

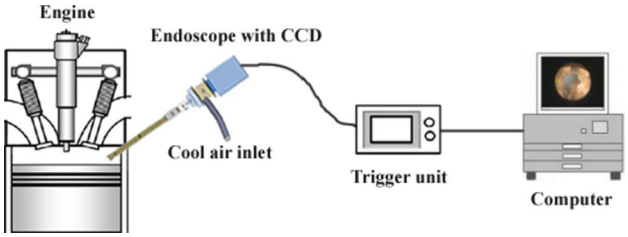

Fig. 3 The schematic diagram of endoscopic measurement

Table 3 Engine test conditions

Description	25% load	50% load
Engine speed (rpm)	1450	1450
Main injection timing (°BTDC)	20	15
Injection pressure (MPa)	85	95
Intake temperature (K)	303	303
Pilot injection timing (°BTDC)	40, 50, 60, 70	
Total injection mass (mg)	15	26
Pilot injection mass (mg)	0, 2.5, 5, 7.5	

obtain accurate picture timing, with an angle encoder. The crank angle corresponding to each picture was converted from the exact time of taking picture recorded by the endoscopic visualization system, and the camera picture processing method described in our previous paper [21].

2.3 Experimental procedure

The engine operating conditions are shown in Table 3. The fuel used in the experiment is 0# diesel, which is sourced from Sinopec. The test procedure was to operate the engine at low speed and loads (1450 r/min, 25% and 50% load), which took a relatively large proportion of emission control in the New European Driving Cycle (NEDC). For reducing the in-cylinder combustion temperature, Exhaust Gas Recirculation (EGR) system was employed, that also decreased inlet oxygen concentration from 21 to 16.5% (25% load) and 17.5% (50% load). The pilot injection mass in percentage of the total injection mass is 0, 16.7%, 33.3%, 50% (25% load) and 0, 9.6%, 19.2%, 28.8% (50% load), respectively. Because the endoscopic visualization system cannot work in high temperature and pressure, 25% load was chosen for visual working operation. From 80 °BTDC to 60 °ATDC, the CCD camera captured pictures per two engine cycles with a step of 0.1° CA, so the interval between every two pictures is 160 ms.

3 Results and discussion

3.1 Effect of pilot injection mass on combustion

Figures 4 and 5 display the effect of injected mass in the pilot injection on the combustion characteristics compared with the single injection. The in-cylinder pressure and HRR are diagramed with different pilot masses. The pilot injection timing was fixed at 40 °BTDC (25% load) and 60 °BTDC (50% load), respectively. It can be concluded from Figs. 4 and 5 that the pilot injection strategies induced higher combustion pressure compared with the single injection. The whole in-cylinder combustion process indicated two stages, that is, the heat release stage of pilot injection and heat release stage of main injection. Moreover, the main combustion started more quickly than single injection. It is mainly because of the in-cylinder thermal conditions by pilot promoted the main injection fuel to burn in advance. As the pilot injection mass raised, the HRR peak value of pilot

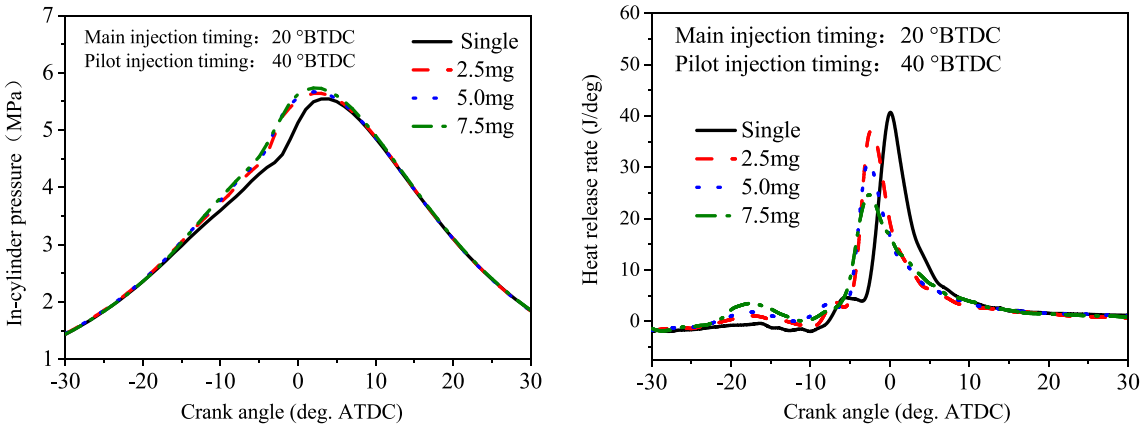

(a) In-cylinder pressure (b) HRR

Fig. 4 In-cylinder pressure and HRR with different pilot injection masses (25% load)

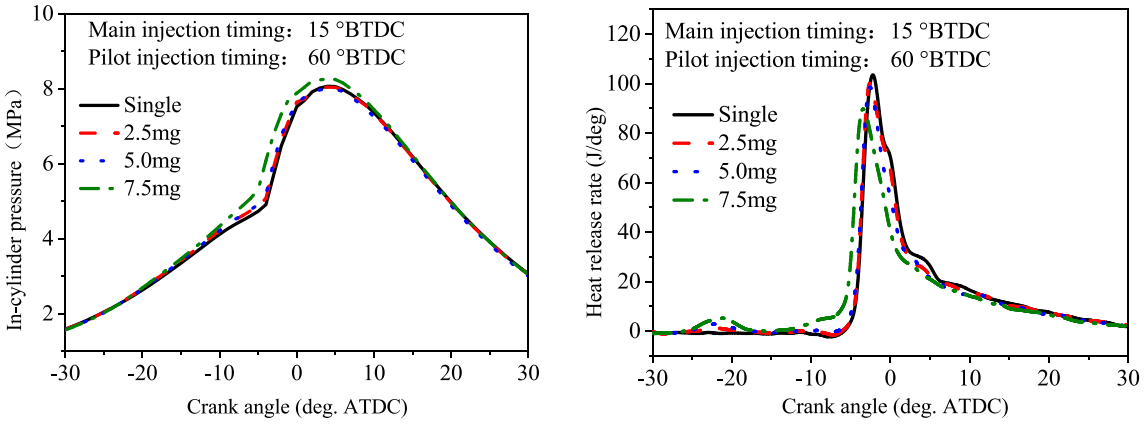

(a) In-cylinder pressure (b) HRR

Fig. 5 In-cylinder pressure and HRR with different pilot injection masses (50% load)

increased. However, the corresponding position remains essentially unaltered. In specific circumstances of engine operation, the in-cylinder temperature and pressure remain comparatively unvaried. Consequently, the initiation of combustion, as influenced by the pilot injection strategy, does not exhibit any significant variation based on alterations in the mass of pilot injection [22]. Additionally, the increase in pilot injection mass caused a decrease in main injection mass, which resulted in lower HRR peak value of main injection.

It can also be observed from Fig. 4 that the pilot mass significantly affected the main combustion. This is due to the fact that, there was some overlap between the main injection duration and the pilot combustion. Similar trend is also found in Fig. 5; however, its effect was small. The pilot-main interval was wider under 50% load condition. Therefore, when the main mass injected into the cylinder, the pilot combustion had finished already. Another reason is possible due to the ratio of pilot mass was less than 25% load.

Figure 6 presents the in-cylinder spray and ignition images under 25% engine load with pilot injection mass, from 20 °BTDC to 4 °BTDC. The first, second, and third row of Fig. 6 corresponds to 2.5, 5.0 and 7.5 mg pilot mass, respectively. In order to analyze conveniently, only the endoscopic viewing area was reserved for all images in the article. It can be noticed that the fuel of all operating conditions has been almost atomized at 12 °BTDC. Diffuse flame did not appear for the pilot mass 2.5 mg, 5.0 mg conditions until 4 °BTDC. However, in case of 7.5 mg, less diffuse flame was found at 8 °BTDC and 4 °BTDC. The combustion temperature before main combustion was greatly promoted by a higher injection mass of pilot, which improved

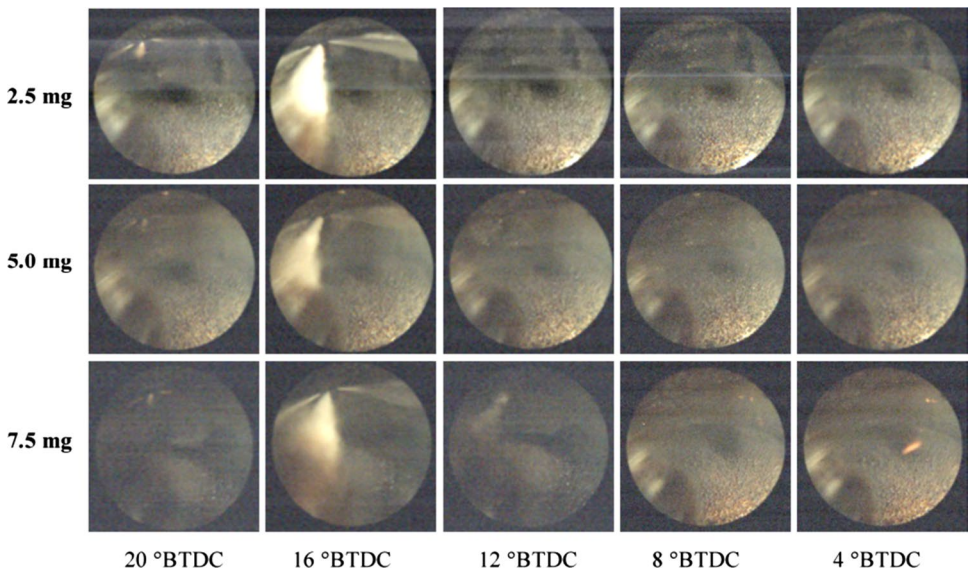

Fig. 6 Spray and ignition images with different pilot masses

the vaporization of main fuel and shortened the premixing time. Thus, the primary cause of diffuse flame is the deficiency of premixing time.

Figure 7 shows the images of flame development at various pilot mass under 25% engine load, from 2 °BTDC to 6 °ATDC. The flame luminance of the first-row images in Fig. 7 is much weaker, and the flame area is small. When the pilot injection increased to 5.0 mg, the flame becomes brighter. A markedly brighter flame appears from 2 °BTDC to 2 °ATDC for the condition with a pilot injection mass of 7.5 mg, and the flame area increases. But the flame becomes dim after 2 °ATDC. Based on the observations of flame images, it can be inferred that the flame area and luminosity experienced an expansion as the mass of pilot injection increased. This can be attributed to the release of a higher amount of heat due to the larger pilot injection mass, subsequently leading to a shortened period of main combustion ignition delay. Therefore, there was an inadequate mixing of fuel and air, which increased the proportion of diffusion combustion. This phenomenon ultimately facilitated the ignition of the main injection [23]. Moreover, this also means higher soot emission. Because flame intensity in the flame image determines by the thermal radiation from the soot particles formed in cylinder [24].

Figure 8 indicates the influences of the pilot injection mass on BSFC. As can be seen from Fig. 8, BSFC first reduces slightly, then increases with the rise of pilot quantity. This is due to pilot-main injection strategy induced the main combustion phase ahead of time, more toward the Top Dead Center (TDC), so BSFC decreased. However, the increase in pilot mass led to more fuel impinging on the wall, this led the BSFC increased. Interestingly, when the pilot injection mass increased from 0 to 5 mg, the BSFC was not significantly increased under 50% engine load, as shown in Fig. 8b. This is due to the main combustion phase was nearly unchanged, because of longer interval between pilot and main injection, and minor ratio of pilot injection mass.

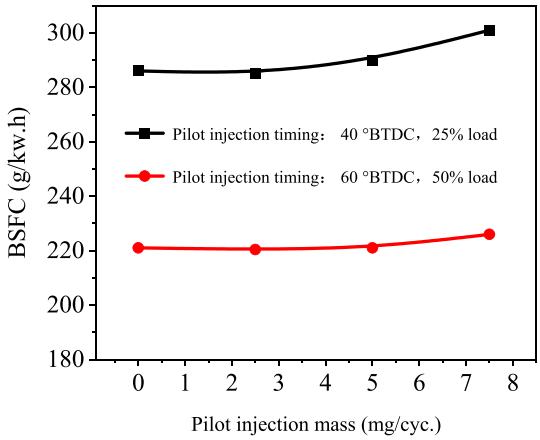

Fig. 8 Influences of pilot injection mass on BSFC

3.2 Effect of pilot injection mass on emissions

The pilot injection strategies have been extensively used to reduce the emission of NO_X. As described in Fig. 9, NO_X emission is obviously reduced compared with single injection. Moreover, NO_X emission reduces with the increase in pilot mass. The maximum reduction rates of NO_X are 54% (25% load) and 25% (50% load), respectively. The information of soot was strongly affected by the fuel–air mixing process of pilot injection. From Fig. 9, it appears that soot emission reduces firstly. This may be due to the reason that increased pilot injection mass could improve the ratio of diffusion combustion, as shown in Fig. 7. Another reason is

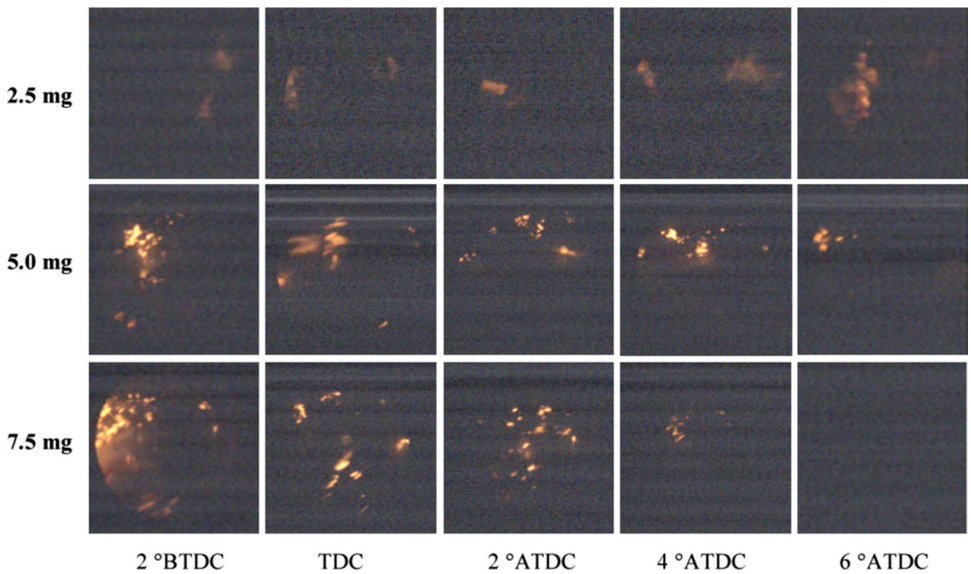

Fig. 7 Combustion process images with different pilot injection masses

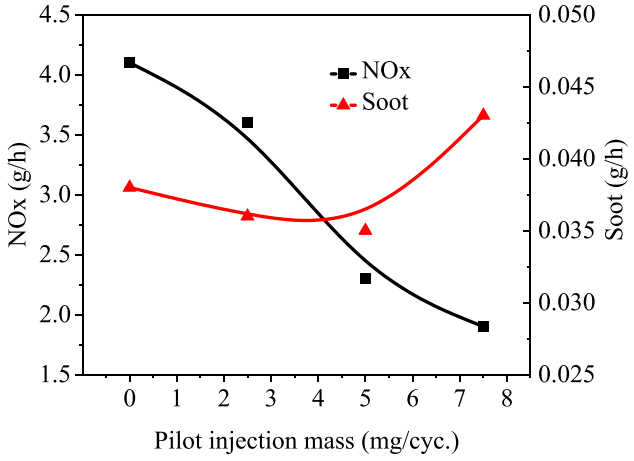

(a) 25% load

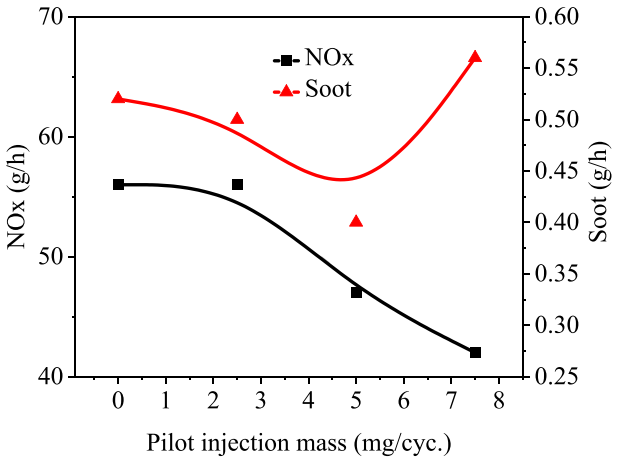

(b) 50% load

Fig. 9 Influences of pilot injection mass on NO_X and Soot emissions

that the pilot combustion had immediate impact on the main combustion, increasing the average in-cylinder pressure and temperature of the main combustion, which is positive on the soot emission reduction. However, as the pilot injection mass increases further, the heat release also increases, leading to a shorter main injection ignition delay. Consequently, the reduced mixing time between fuel and air results in an uneven air/fuel mixture, leading to increased soot emissions [25]. Additionally, the increased pilot mass causes more fuel to impinge on the wall and shortens the ignition delay of the main injection, thereby negatively affecting the air–fuel mixture. Therefore, the finally generated soot was rise.

3.3 Effect of pilot injection timing on combustion

The effect of pilot injection timings on the in-cylinder pressure and HRR is shown in Figs. 10 and 11. The pilot injection mass is 5 mg, and the main injection timing was set to 20 °BTDC (25% load), 15 °BTDC (50% load), respectively. It can be concluded from Figs. 10 and 11 that pilot injection resulted in higher peak in-cylinder pressure and lower peak HRR than single injection. For instance, in the cases of 25% load shown in Fig. 10a, with the pilot injection timing advanced from − 40 °BTDC to − 70 °BTDC, the peak in-cylinder combustion pressure was increased and its corresponding crank angle moved ahead, and the main combustion process was obviously accelerated. The observed phenomenon can be attributed to the increase in fuel-gas mixing time caused by the earlier pilot injection. This increase is beneficial for the formation of the ignited mixture and accelerates the combustion speed [26]. Additionally, the main injection timing (20 °BTDC) was approached the peak of pilot combustion. This can be seen from the first peak HRR curves depicted in Fig. 10a. Consequently, the combustion performance was improved.

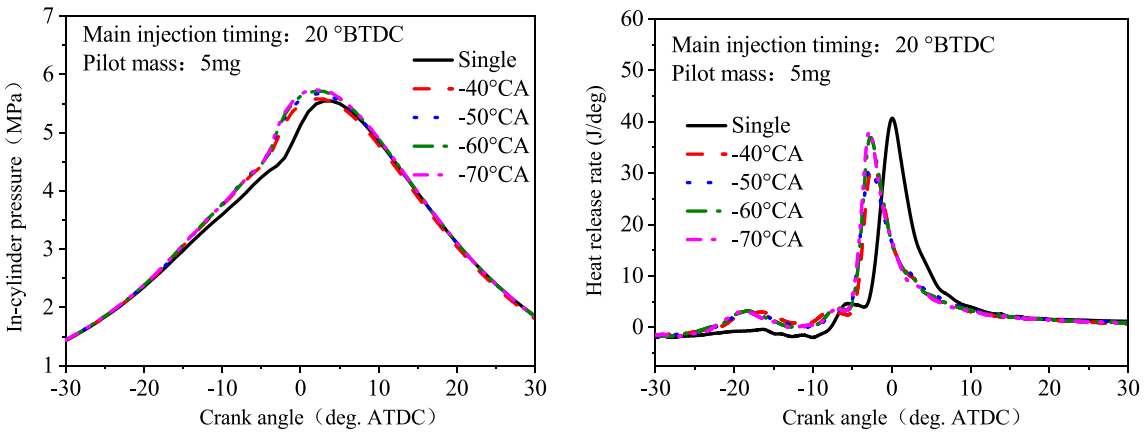

(a) In-cylinder pressure (b) HRR

Fig. 10 In-cylinder pressure and HRR with different pilot injection timings (25% load)

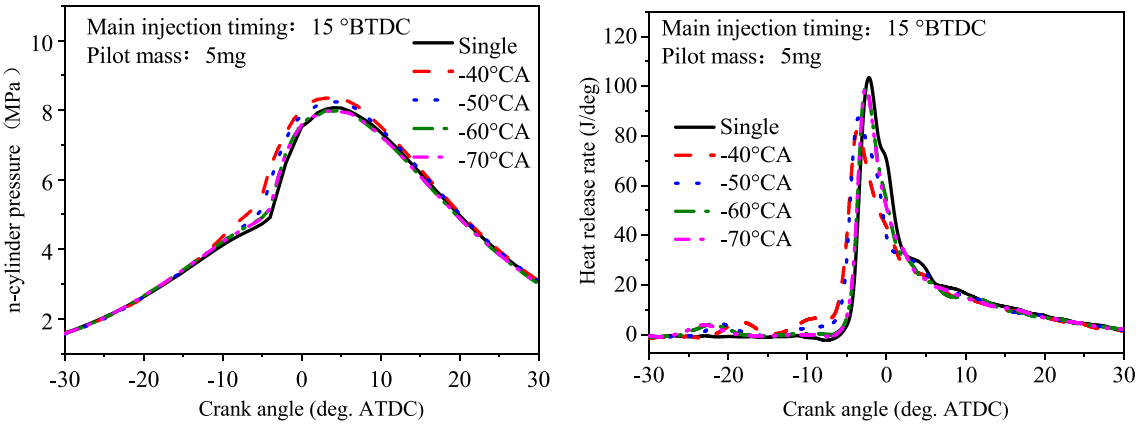

(a) In-cylinder pressure (b) HRR

Fig. 11 In-cylinder pressure and HRR with different pilot injection timings (50% load)

In the cases of 50% load shown in Fig. 11b, with advanced injection timing of pilot, the in-cylinder pressure was decreased, and the main combustion showed lower heat release rate. The reason is that the combustion process of the pilot fuel was finished at about 17 °BTDC, except the pilot injection timing of 40 °BTDC. The earlier the end of the pilot fuel combustion, the less impact on the main injection fuel combustion process.

Figure 12 depicts the combustion images at various pilot timings by endoscopic visualization under 25% engine load, with a constant pilot mass condition (5 mg). It can be seen that luminous flames were not observed at CA5. The first appearance time of luminous flame advanced from 4.2 °BTDC to 4.8 °BTDC with the advance of pilot injection timing, and the area of luminous flame zone increased. And the flame luminance becomes higher when the pilot injection timing advanced from 40 °BTDC to 60 °BTDC, which shows that advanced pilot injection timing results in higher in-cylinder pressure and temperature before main injection, causing shorter ignition delay of main combustion. However, the flame luminance remains almost the same when the pilot timing advanced to 70 °BTDC. This indicates that premature pilot injection timing has a limited effect on main combustion. Moreover, it can be seen from the images of CA10, CA50, and CA90 that earlier pilot injection timing exhibits longer combustion duration. Here, CA5, CA10, CA50, and CA90 are defined as the crank angles at which 5%, 10%, 50%, and 90% of total heat released.

Figure 13 represents the effect of the pilot injection timings on BSFC. With the advance of pilot injection timings, BSFC at 25% load notably increased. As mentioned above, the main fuel was sprayed in the combustion process of pilot fuel, so the combustion phase is advanced away from the TDC, and the combustion efficiency decreases. However, for 50% load conditions, it is the other way round. This is primarily because the main injection occurs behind the pilot combustion, as shown in Fig. 11b.

3.4 Effect of pilot injection timing on emissions

Figures 14 and 15 show the effects of pilot injection timing on NO_X and soot emission at 25% and 50% load. As can be seen in Fig. 14, the NO_X emissions are lower than single injection. Additionally, with the advance of pilot injection timing, more NO_X emissions were exhausted. It is mainly due to the fact that an earlier combustion phase was caused by the pilot fuel. Moreover, more mixture of fuel and air were transported into the premixed combustion process and HRR was increased. As a result, the combustion temperature in-cylinder increased, and this may be due to that NO_X formation increases with advanced pilot injection timing. Figure 15 indicates the effects of pilot injection timings on the soot emissions. It could be concluded that pilot injection could improve the soot emissions. Nevertheless, when pilot injection timing was advanced more than 60 °BTDC, the exhausted soot emission approximately remained constant or even increased. This could be attributed to advancing pilot injection timing resulted in more fuel impinging on the wall. This is the same reason why the soot emissions at 7.5 mg conditions are higher than single injection.

3.5 Optimization

In this section, we utilize response surface methodology (RSM) to optimize the pilot injection parameters. RSM is a mathematical and statistical method [27] employed to optimize the response affected by multiple independent variables. Equation (1) represents a second-order polynomial equation used to predict the output response while considering the input factors.

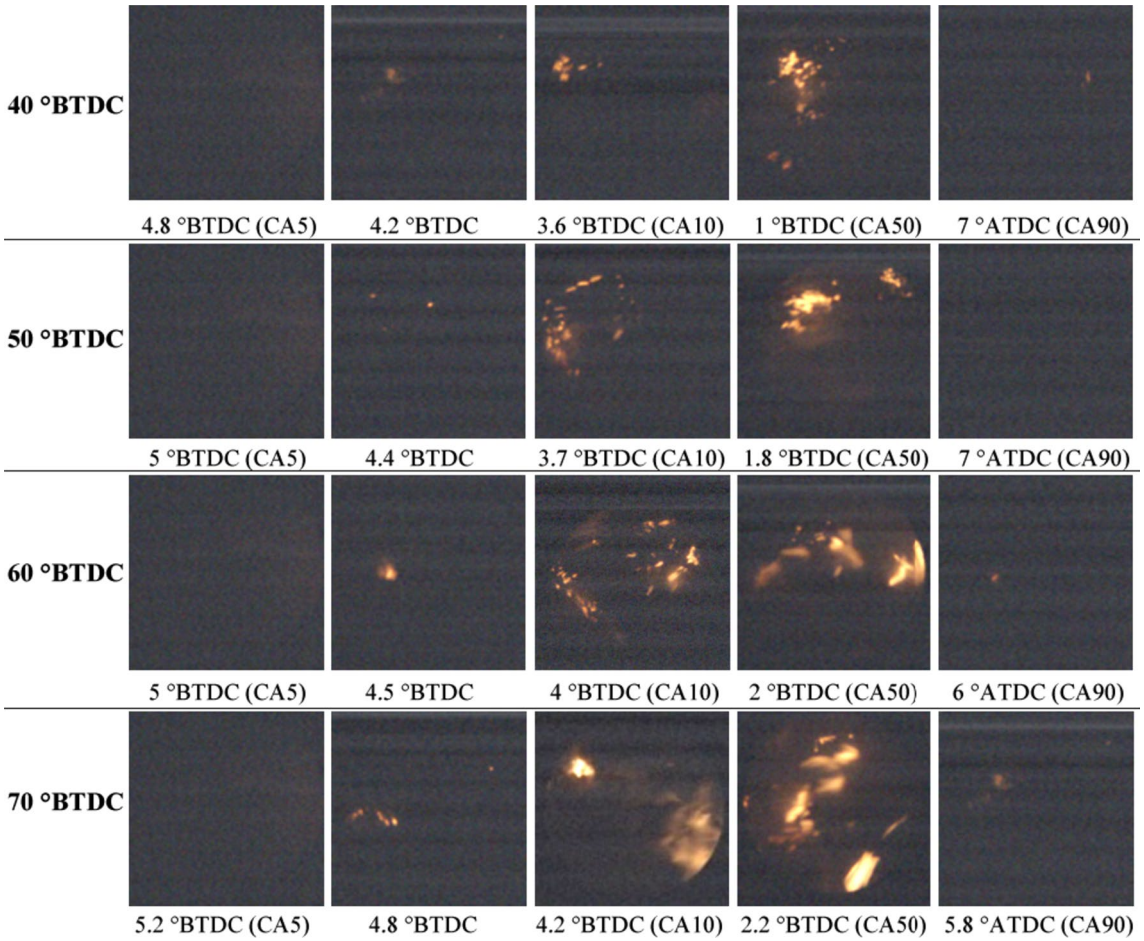

Fig. 12 Combustion process images under different pilot injection timings

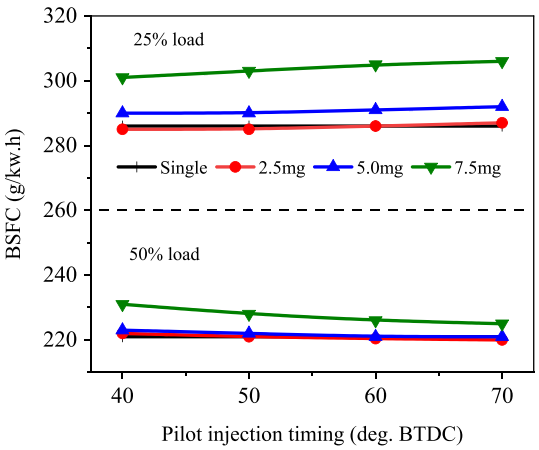

Fig. 13 Effect of pilot injection timing on BSFC

$$Y = b_0 + \sum_{i=1}^{k} b_i x_i + \sum_{i=1}^{k} b_{ii} x_i^2 + \sum_{i=1, j=i+1}^{k} b_{ij} x_i x_{ij} + \varepsilon \quad (1)$$

In Eq. (1), Y represents the response, x_i and x_{ij} denote the input parameters, b_0 corresponds to the constant coefficient, k indicates the number of factors, b_i, b_{ii} and b_{ij} represent the regression coefficients, and ε represents the unanticipated error.

The optimization process is illustrated with an example of 25% load. Design-Expert 8.0 software was selected to apply RSM. The input variables were pilot injection mass (0, 2.5, 5, 7.5 mg) and timing (40, 50, 60, 70 °BTDC). The response variables were BSFC (g/kW. h), NO_X (g/h) and Soot (g/h). Table 4 displays the ANOVA results, which confirm the validity of the RSM models through the values of R^2, adjusted R^2, and predicted R^2. Figure 16 presents the normal probability plots of residual for the responses, indicating that the data points are nearly distributed in a straight line, and the errors follow a normal distribution, thus validating the credibility of the RSM models.

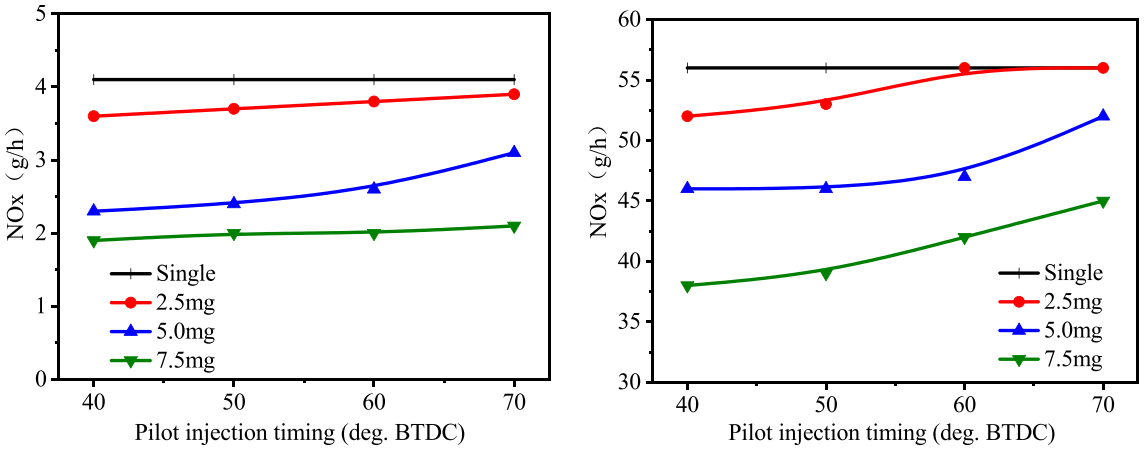

Fig. 14 Effect of pilot injection timing on NO_X

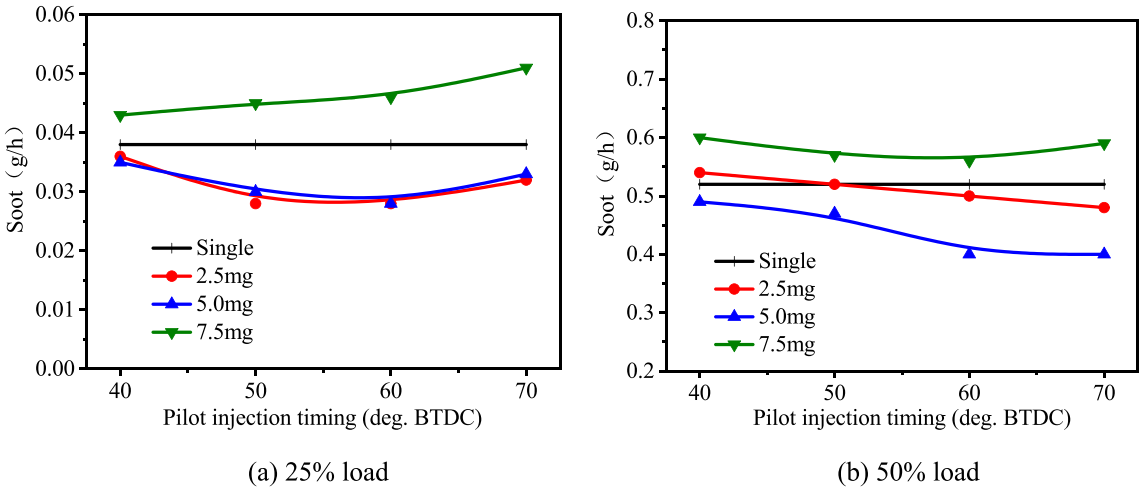

Fig. 15 Effect of pilot injection timing on Soot

Table 4 Results of ANOVA

Factors	R^2	Adjusted R^2	Predicted R^2
BSFC	0.9964	0.9945	0.9914
NO_X	0.9938	0.9845	0.9409
Soot	0.9969	0.9832	0.8083

Figure 17 shows the interactive impacts of the pilot injection mass and timing on BSFC. BSFC is lowest at about 2.5 mg pilot injection mass and then rises rapidly with the increase in pilot injection mass. It is worth noting that at a retarded pilot injection timing, the BSFC is more affected by pilot injection mass at 50% load.

Figure 18 illustrates the interactive impacts of pilot injection mass and timing on NO_X. Similar to BSFC, NO_X is significantly influenced by the pilot injection mass, but the trends exhibit an opposite contrast: NO_X experiences a sharp decrease as the pilot injection mass increases. The minimum NO_X values are depicted in Fig. 18, corresponding to 1.9 g/h (25% load) and 38 g/h (50% load), achieved with a pilot injection mass of 7.5 mg and a pilot injection timing of 40 °BTDC. Figure 19 shows the interactive effects of pilot injection mass and timing on soot emission. According to the graphs, at 25% load, soot initially decrease sharply but then increase as both pilot injection mass and timing rise. However, at 50% load, pilot injection timing has weak impact on soot emissions when compared to the influence of pilot injection mass.

Optimizing the pilot injection mass and timing was crucial due to the trade-off between BSFC and emissions. The desirability profile and its functions were utilized for

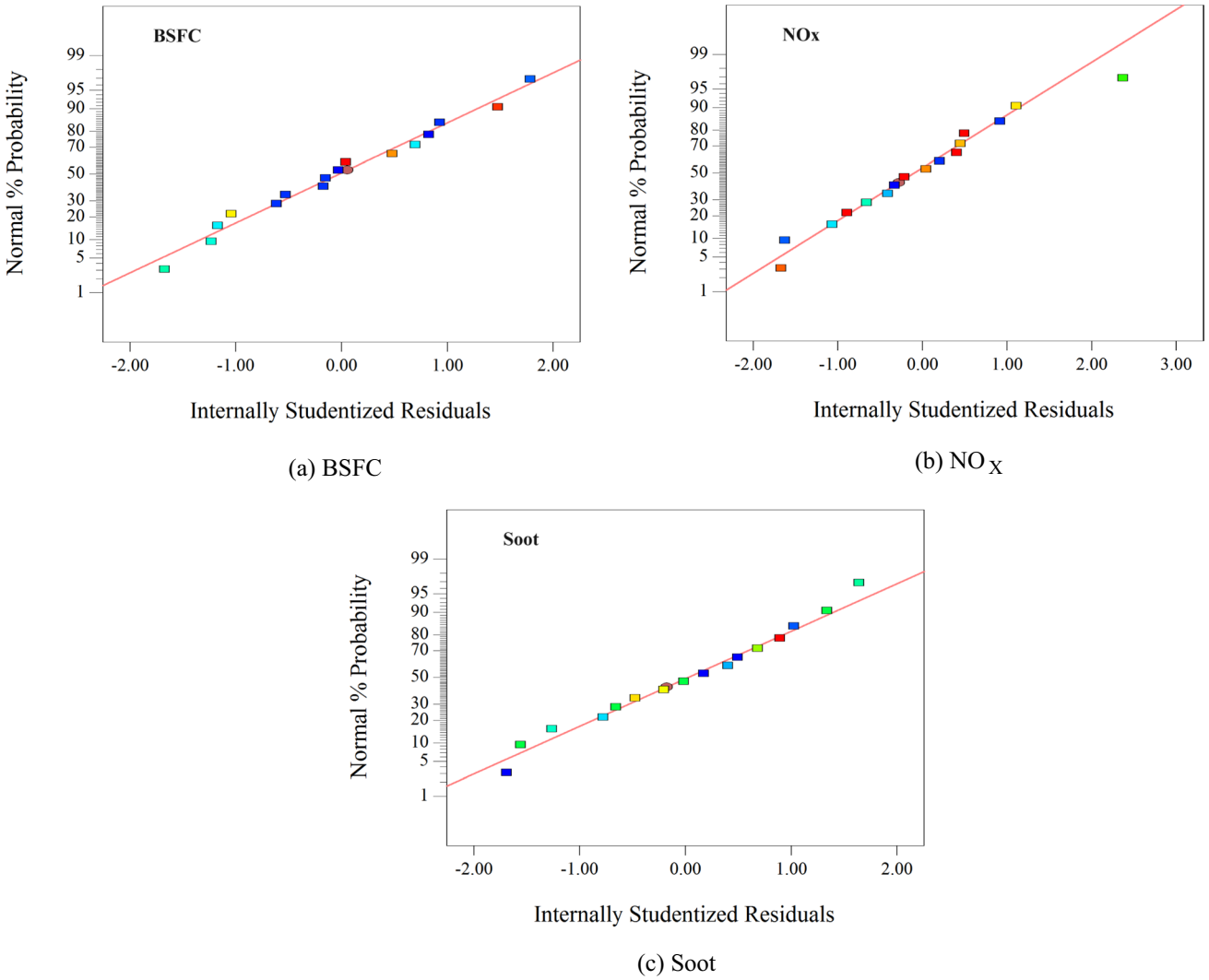

Fig. 16 Normal probability plot of the residual for the composite for responses

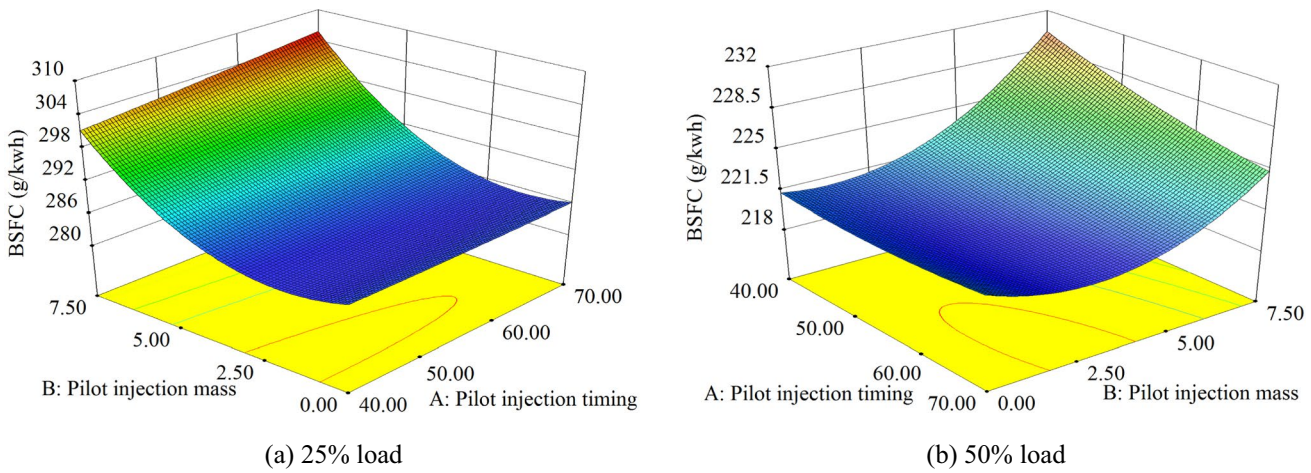

Fig. 17 Interaction of pilot injection mass and timing on BSFC

optimization. Multiple best solutions were obtained using the desirability-based approach. At 25% load, the pilot injection parameters of 50 °BTDC for pilot injection timing and 4.4 mg for pilot injection mass yielded the maximum desirability of 0.799. Similarly, at 50% load, the optimal responses were achieved with pilot injection timing of 58.9 °BTDC and pilot injection mass of 5.5 mg, resulting in a maximum desirability of 0.681.Validation experiments were conducted to assess the accuracy of the RSM optimal responses, and the results are shown in Table 5, demonstrating the reliability of the optimization analysis. Comparing the experimental results with single injection in Figs. 13, 14 and 15, the improvements at 25% load included a 36.34% decrease in NO_X and a 23.68% decrease in Soot, with only a marginal 1.39% increase in BSFC. At 50% load, there were reductions of 0.45% in BSFC, 8.92% in NO_X, and 11.53% in Soot.

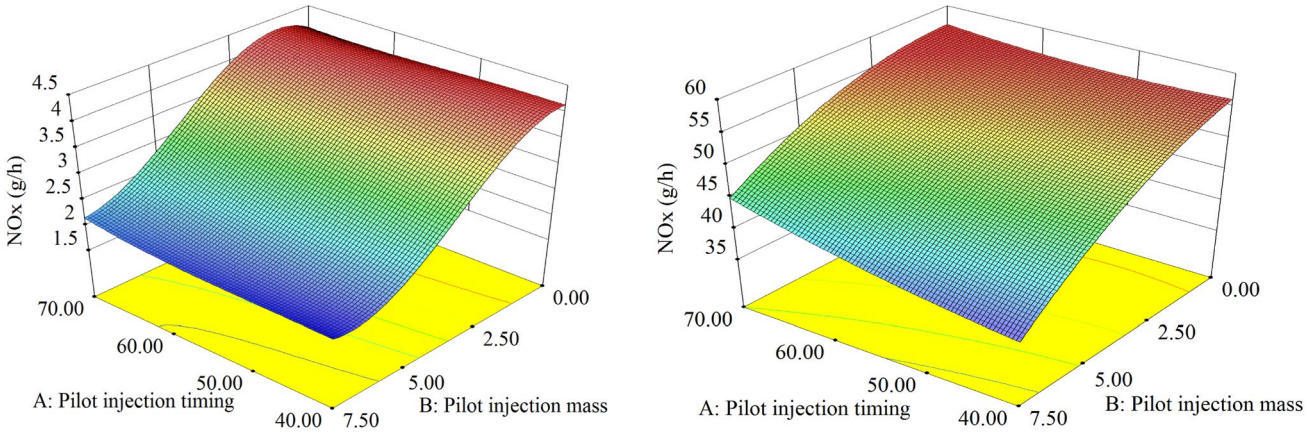

(a) 25% load (b) 50% load

Fig. 18 Interaction of pilot injection mass and timing on NO_X

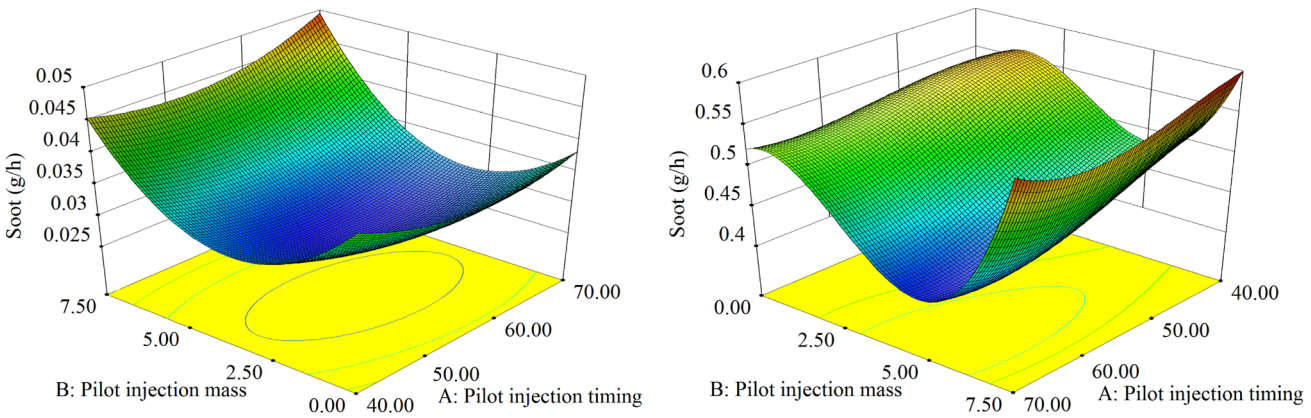

(a) 25% load (b) 50% load

Fig. 19 Interaction of pilot injection mass and timing on Soot

Table 5 RSM and experimental results

Load	Predicted		Experiment		Error%	
	25%	50%	25%	50%	25%	50%
BSFC	288.77	222.34	290	220	0.42	1.06
NO_X	2.74	47.46	2.61	51	4.98	6.94
Soot	0.028	0.418	0.029	0.46	3.45	9.13

4 Conclusions

In the current work, the effects of pilot injection on the combustion process and emission of a PCCI diesel engine equipped with an endoscopic visualization system were researched. The main conclusion is as follows:

(1) The increase in pilot injection mass results in a stronger flame luminance near TDC and the expansion of the flame area. However, after TDC, the flame luminance rapidly decreases. As the pilot injection timing advanced from 40 to 60 °BTDC, the first appearance time of the flame becomes earlier, and the flame luminance increases. Nevertheless, when the pilot injection timing is advanced to 70 °BTDC, the flame luminance remains almost the same. Moreover, earlier pilot injection timing exhibits longer combustion duration.

(2) The BSFC increases with the increase in pilot injection mass, soot decreased firstly and increased secondly, and the maximum reduction in NO_X is 54%. With the advancement of pilot injection timing, NO_X levels increase, the BSFC gets worse at 25% load, and at the same load, there is a decrease in soot initially, followed by an increase. Interestingly, at 50% load, there is a gradual decrease in Soot.

(3) By optimizing the pilot injection strategy, compared to single injection, NO_X and Soot decreased by 36.34% and 23.68%, respectively, at 25% load, with a weak increase in BSFC. At 50% load, BSFC, NO_X, and soot were reduced 0.45%, 8.92%, and 11.53%, respectively.

Funding This study is supported by the Natural Science Foundation of Jiangsu Province, China (Grant No. BK20201166), and the Graduate student innovation fund project of Jiangsu province (KYLX16_0890).

Declarations

Conflict of interest The authors declare that there is no conflict of interest.

References

1. Fan X, Dai J, Lu J et al (2020) Kinetic behavior evaluation of electromagnetic valve train subject to exhaust gas force. Appl Therm Eng 171:115097
2. Shim E, Park H, Bae C (2020) Comparisons of advanced combustion technologies (HCCI, PCCI, and dual-fuel PCCI) on engine performance and emission characteristics in a heavy-duty diesel engine. Fuel 262:116436
3. Singh AP, Kumar V, Agarwal AK (2020) Evaluation of comparative engine combustion, performance and emission characteristics of low temperature combustion (PCCI and RCCI) modes. Appl Energy 278:115644
4. d'Ambrosio S, Ferrari A, Mancarella A (2022) Time frequency analysis for the evaluation of ignition delay in conventional and PCCI combustion modes. Therm Sci Eng Prog 33:101352
5. Bharadwaz YD, Kumari AS (2023) PCCI combustion of low-carbon alternative fuels: a review. J Therm Anal Calorim 148(12):5179–5207
6. Lu Y, Fan C, Chen Y et al (2023) Effect of injection strategy optimization on PCCI combustion and emissions under engine speed extension in a heavy-duty diesel engine. Fuel 332:126053
7. Jia M, Xie M, Wang T et al (2011) The effect of injection timing and intake valve close timing on performance and emissions of diesel PCCI engine with a full engine cycle CFD simulation. Appl Energy 88(9):2967–2975
8. Zehni A, Balazadeh N, Hajibabaei M et al (2020) Numerical study of the effects of split injection strategy and swirl ratio for biodiesel PCCI combustion and emissions. Propuls Power Res 9(4):355–371
9. Zhang Y, Jia M, Liu H et al (2014) Development of a new spray/wall interaction model for diesel spray under PCCI-engine relevant conditions. At Sprays 24(1):41–80
10. Horibe N, Harada S, Ishiyama T, Shioji M (2009) Improvement of premixed charge compression ignition based combustion by two-stage injection. Int J Eng Res 10:71–80
11. Ge JC, Wu G, Choi NJ (2022) Comparative study of pilot–main injection timings and diesel/ethanol binary blends on combustion, emission and microstructure of particles emitted from diesel engines. Fuel 313:122658
12. Cao J, Leng X, He Z, Wang Q et al (2019) Experimental study of the diesel spray combustion and soot characteristics for different double-injection strategies in a constant volume combustion chamber. J Energy Inst 93:335–350
13. Herfatmanesh MR, Lu P, Attar MA et al (2013) Experimental investigation into the effects of two-stage injection on fuel injection quantity, combustion and emissions in a high-speed optical common rail diesel engine. Fuel 109:137–147
14. Qiu L, Cheng X, Liu B et al (2016) Partially premixed combustion based on different injection strategies in a light-duty diesel engine. Energy 96:155–165
15. Torregrosa AJ, Broatch A, García A et al (2013) Sensitivity of combustion noise and NOx and soot emissions to pilot injection in PCCI Diesel engines. Appl Energy 104:149–157
16. Wang J, Jin Y, Zhang YT et al (2020) Multiple injection distribution of electronically controlled injector in typical working conditions of diesel engine. Autom Eng 42(2):157–163, 177
17. Huang H, Huang R, Guo X et al (2019) Effects of pine oil additive and pilot injection strategies on energy distribution, combustion and emissions in a diesel engine at low-load condition. Appl Energy 250:185–197
18. Ehleskog R, Ochoterena RL, Andersson S (2007) Effects of multiple injections on engine-out emission levels including particulate mass from an HSDI diesel engine. SAE paper 2007-01-0910
19. d'Ambrosio S, Ferrari A (2015) Potential of double pilot injection strategies optimized with the design of experiments procedure to improve diesel engine emissions and performance. Appl Energy 155:918–932
20. Catapano F, Iorio SD, Luise L et al (2019) Influence of ethanol blended and dual fueled with gasoline on soot formation and particulate matter emissions in a small displacement spark ignition engine. Fuel 245:253–262
21. Xu H, Yin B, Liu S et al (2017) Visualization of combustion performance and emission characteristics of a four-cylinder diesel engine at various injection timings and engine loads. J Braz Soc Mech Sci Eng 39(10):3757–3767

22. Li J, Liu J, Ji Q et al (2022) Effects of pilot injection strategy on in-cylinder combustion and emission characteristics of PODE/methanol blends. Fuel Process Technol 228:107168
23. Hu J, Yao C, Geng P et al (2018) Effects of pilot injection strategy of diesel fuel on combustion characteristics in a premixed methanol-air mixture atmosphere in a CVCC. Fuel 234:1132–1143
24. Jiotode Y, Agarwal AK (2016) In-cylinder combustion visualization of Jatropha straight vegetable oil and mineral diesel using high temperature industrial endoscopy for spatial temperature and soot distribution. Fuel Process Technol 153:9–18
25. Huang H, Liu Q, Yang R et al (2015) Investigation on the effects of pilot injection on low temperature combustion in high-speed diesel engine fueled with n-butanol–diesel blends. Energy Convers Manag 106:748–758
26. Su X, Chen H, Gao N et al (2023) Combustion and emission characteristics of diesel engine fueled with diesel/cyclohexanol blend fuels under different exhaust gas recirculation ratios and injection timings. Fuel 332:125986
27. Xu H, Fan X (2023) High altitude performance optimization of diesel engine fueled with biodieselmethanol blends using response surface methodology. J Mech Sci Technol 37:1–9